Performance Analysis of Four-Bed H_2 PSA Process Using Layered Beds

Jong-Ho Park, Jong-Nam Kim, and Soon-Haeng Cho
Korea Institute of Energy Research, Yusungku, Taejon 305-343, Korea

Hydrogen purification from a typical cracked gas mixture ($H_2/CO_2/CH_4/CO$) by the four-bed PSA process was studied experimentally and theoretically using layered bed of activated carbon and zeolite 5A. The mathematical model accounts for the mass and heat transfer resistance using the linear driving force approximation for the particle uptake, and the ideal adsorbed solution model represents the multicomponent adsorption equilibrium. Effects of the superficial velocity, heat transfer resistance and the bed layering on the process performance were investigated. Since the recovery sharply decreases above a certain productivity at the given purity, the relation between the productivity and recovery was studied before the process design. Its performance decreased with the increase in heat transfer resistance, but increased with heat transfer resistance in some range. Both the experiment and theory showed optimum carbon-to-zeolite ratios. Those optimum ratios depend on such operating variables as the superficial velocity, heat transfer resistance and product purity. For higher product purity more zeolite was used. As the superficial velocity increased, the process performance has its maximum at higher carbon-to-zeolite ratio. Except for the adiabatic conditions, the optimum carbon-to-zeolite ratio increased with the increase in the heat transfer resistance. At the adiabatic conditions, however, the optimum carbon-to-zeolite ratio was lower than that at the nonisothermal conditions.

Introduction

Adsorption has become an important tool for gas separation, particularly by pressure swing adsorption (PSA). The applications of PSA include air separation, gas drying, hydrogen purification, *n*-paraffin separation, argon recovery, and so on (Yang, 1987; Ruthven et al., 1994).

Hydrogen is largely produced by steam reforming of naphtha or methane followed by PSA separation. The reformer effluent gas contains $H_2/CO_2/CH_4/CO$ and small amounts of water. No adsorbent removes all the impurities equally well. Some adsorbents are suitable to remove a specific impurity. For example, zeolite is more suitable than activated carbon to remove carbon monoxide. On the other hand, methane is more easily removed by the activated carbon. So, to purify hydrogen from the reformer effluent gas, two or more adsorbents are used simultaneously. Water vapor and carbon dioxide are strongly adsorbed on the zeolite, so that they are not easily desorbed by reducing the pressure and tend to accumulate in the zeolite. Therefore, they are removed before they contaminate the zeolite. Water vapor is usually removed by the silica gel or activated alumina, and carbon dioxide is removed by the activated carbon. All the adsorbents are packed in a bed altogether rather than packed in a separate bed for process simplicity (Yang, 1987).

The idea of using layered beds consisting of different sorbents for cyclic adsorption/ion exchange is not new (Feldbauer, 1967; Wagner, 1969; Klein and Vermeulen, 1975; Frey, 1983; Wankat and Tondeur, 1985; Chlendi and Tondeur, 1996; Watson et al., 1996; Malek and Farooq, 1998). The basic principle is to use a weak sorbent at the inlet section of the bed followed by stronger sorbents in order to maximize the use of each sorbent and, hence, minimize the adsorber size. Even though the idea has been introduced long before, the theoretical analysis for the PSA process using layered beds appears in recent years. Chlendi and Tondeur

Correspondence concerning this article should be addressed to J. N. Kim.

(1995) studied concentration wave refraction, dispersion, and interference phenomena occurring in the layered beds using the pseudo-characteristic method. Chlendi et al. (1995) performed the sensitivity analysis for the H_2 PSA process using layered beds with the isothermal and nonequilibrium model. Their analysis showed the effects of the operating and design variables such as the column length and feed velocity on the process performance. Even though the results are useful to understand the process dynamics, it is hard to obtain the optimum design and operating conditions from the results. Pigorini and LeVan (1997) studied the single component purification in layered beds using a four-step PSA cycle. Isothermality, constant fluid velocity, and frozen solid approximation were assumed in their analysis. They showed that the process performance depends on the relative length of each layer even in the single component adsorption. Tanczyk and Warmuzinski (1997, 1998) developed nonisothermal, nonequilibrium, and nonadiabatic models for the H_2 PSA process using layered beds. They paid attention to the development of a proper model to predict the experimental results from the large scale of H_2 PSA. Lee et al. (1999) dealt the hydrogen purification from the coke oven gas using the layered beds of activated carbon and zeolite 5A. They showed that the product purity depended on the carbon-to-zeolite ratio. They defined the optimum carbon-to-zeolite ratio as the ratio that gave the highest product purity. However, the real optimum carbon-to-zeolite ratio is not sought by the above definition since the other quantities characterizing the process performance are not considered. Three quantities define the process performance of the PSA process: the product purity, recovery, and productivity. At the optimum carbon-to-zeolite ratio, the process has to give the highest product recovery and productivity at the given product purity.

This article presents the experimental results on the four-bed H_2 PSA process using layered beds and the theoretical prediction from the nonisothermal and nonequilibrium model. For simplicity, we assume that the moisture of the reformer effluent gas is completely removed in a separate unit. The mathematical model adopts the ideal adsorbed solution (IAS) model to represent the multicomponent adsorption equilibrium. The optimum carbon-to-zeolite ratio (carbon layer height/zeolite layer height) will be identified by comparing the recovery and productivity at the given purity. The effects of the superficial velocity and heat-transfer resistance on the process performance and the optimum carbon-to-zeolite ratio will be investigated.

Experimental PSA Unit and Cycle Sequence

The adsorbents used in this study were activated carbon and zeolite molecular sieve 5A. The activated carbon was supplied by Calgon Corporation (C30-53) with a pellet size of 3 mm. The 5A zeolite was supplied by CECA (siliporite NK 20) with a pellet size of 1.6 mm. The physical properties of the adsorbents and bed are listed in Table 1.

Figure 1 shows the 4-bed H_2 PSA process. The bed was fabricated from the stainless steel pipe of 2.46 cm ID, 120 cm length, and 0.5 cm wall thickness, and it was divided into four sections to facilitate changing the height of each adsorbent layer. The ten thermocouples were installed at one of the four columns in order to track the thermal wave front. A product storage vessel was installed at the product end and from which the product backfill gas was supplied. The rates of pressurization, purge, and pressure equalization were controlled by the hand control valve. The product concentration and flow rate are monitored continuously and automatically with a mass spectrometer (BALZERS MSC-200 AutoCube) and a mass-flow meter, respectively. The sampling port was placed downstream of the mass-flow meter so that the product flow rate could be measured without any loss due to sampling. The adsorption pressure was fixed at 23.6 atm with the back pressure regulator. The control of the solenoid valve switching and the data acquisition of measuring variables were done by a PLC (Siemens) linked to a person computer, which was installed FIX DMACS software. The PC monitor provided an on-line display of the dynamic changes in all the measured values. It was judged that the process reached cyclic steady state when the concentration difference between two subsequent cycles was less than 0.005%. It required 30 to 50 cycles.

Table 1. Parameters Used in the Simulations

		Activated Carbon	Zeolite 5A
Physical Properties of Bed and Adsorbents			
Bed inner dia.	(cm)	2.46	
Bed outer dia.	(cm)	3.4	
Bed density	(g/cm^3)	0.544	0.691
Bed porosity		0.36	0.36
Particle density	(g/cm^3)	0.85	1.08
Density of wall	(g/cm^3)	8.0	
Heat capacity of gas	($cal/mol \cdot K$)	8.0	
Heat capacity of ads.	($cal/g \cdot K$)	0.21	0.23
Heat capacity of wall	($cal/g \cdot K$)	0.11	
Total bed length	(cm)	120	
Mass- and Heat-Transfer Coefficients			
h_w (ads. step)	($cal/cm^2 \cdot s \cdot K$)	3.3×10^{-3}	1.8×10^{-3}
h_w^o	($cal/cm^2 \cdot s \cdot K$)	1.0×10^{-3}	1.0×10^{-3}
U_w	($cal/cm^2 \cdot s \cdot K$)	1.0×10^{-3}	
k_{CO_2}	(s^{-1})	0.1	0.1
k_{CO}	(s^{-1})	0.3	0.15
k_{CH_4}	(s^{-1})	0.4	0.2
k_{H_2}	(s^{-1})	1	1

The cycle sequences studied are as follows: (I) adsorption (AD); (II) first pressure equalization (EQ I-BD); (III) provide purge (PP); (IV) second pressure equalization (EQ II-BD); (V) blow down (BD); (VI) purge (PU); (VII) second pressure equalization (EQ II-PR); (VIII) first pressure equalization (EQ I-PR); (IX) back fill (BF). The cycle sequence is given in Figure 2. For all the experiments, premixed gas mixtures of composition H_2: 72.36%, CO_2: 21.18%, CO: 2.49%, CH_4: 3.97% were used. The main parameters studied experimentally are the effects of the height of activated carbon layer and feed velocity. The experimental operating conditions are summarized in Table 2. In these cycles, the amount of purge is determined by the decrease of the pressure during the PP step. The larger the decrease of the pressure, the more quantity is used in the purge. At every experimental run, the duration of pressure equalization steps was set to 6 s and the decrease of the pressure during the PP step was 3 atm. As shown in Table 2, adsorption time was varied from 35 s to 90 s. With the change of the adsorption step time, the step times of purge, provide purge (PP) and backfill steps were changed.

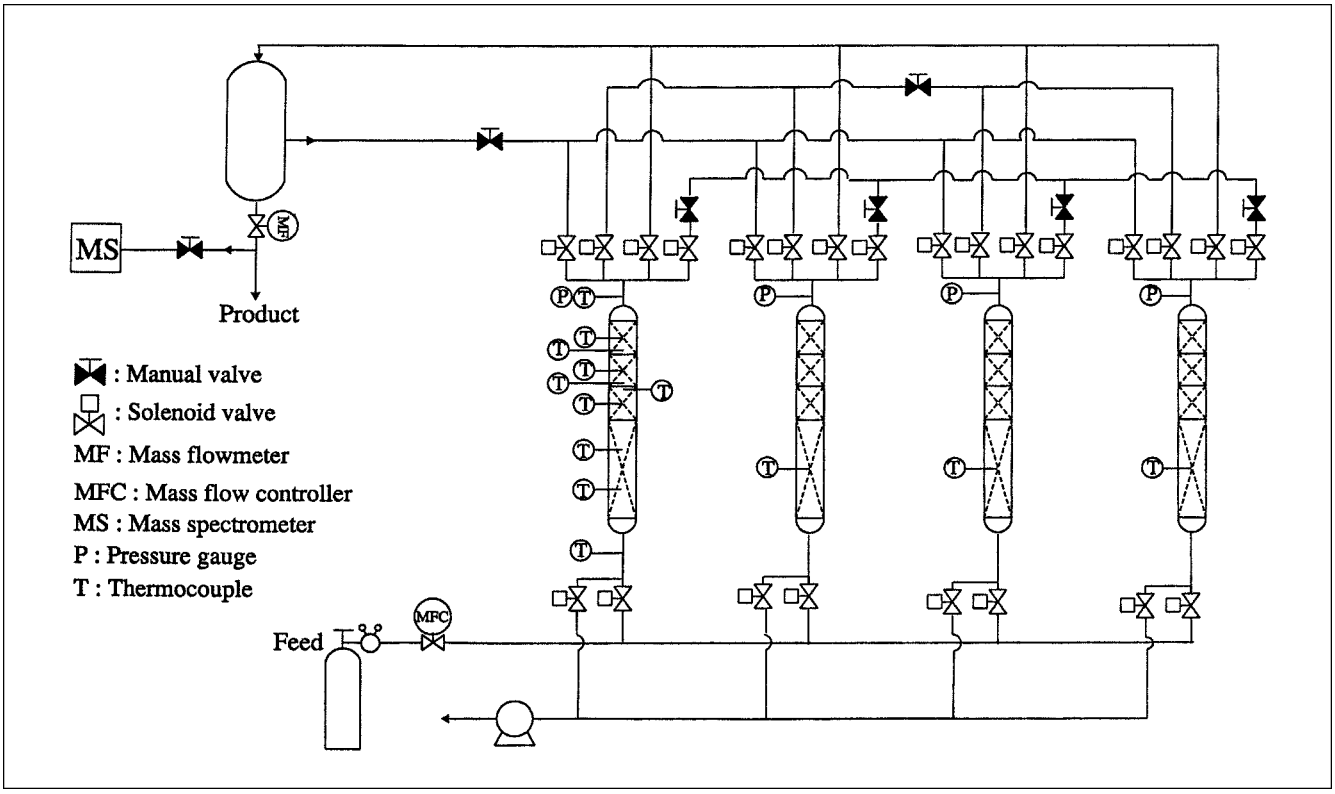

Figure 1. Four-bed H_2 PSA.

Mathematical Model

The mathematical model adopted is a nonisothermal, nonequilibrium, bulk separation model with a nonlinear multicomponent equilibrium isotherm (the IAS theory). The assumption used to derive the model included the following: ideal gas behavior; negligible axial pressure gradient; no radial gradient; no axial dispersion and no axial heat conduction; thermal equilibrium between the gas phase and the adsorbents. Mass transfer is represented by the linear driving force (LDF) approximation.

Based on the above assumptions, the mass balance for each component of the mixture and the total mass balance are written as follows

Component mass balance

$$\frac{\partial y_i}{\partial t} + u\frac{\partial y_i}{\partial z} + \frac{(1-\epsilon)}{\epsilon}\rho_p \frac{RT}{P}\frac{\partial \bar{q}_i}{\partial t} - y_i \sum_j \frac{(1-\epsilon)}{\epsilon}\rho_p \frac{RT}{P}\frac{\partial \bar{q}_j}{\partial t} = 0 \quad (1)$$

Total mass balance

$$\frac{\partial C}{\partial t} + \frac{\partial (uC)}{\partial z} + \sum_i \frac{1-\epsilon}{\epsilon}\rho_p \frac{\partial \bar{q}_i}{\partial t} = 0 \quad (2)$$

Mass transfer is expressed by the LDF approximation

$$\frac{\partial \bar{q}_i}{\partial t} = k_i(q_i^* - \bar{q}_i) \quad (3)$$

Energy balance for the gas phase includes the heat transfer to the column wall

$$\left(\epsilon c_{pg} C + (1-\epsilon)c_{ps}\rho_p\right)\frac{\partial T}{\partial t} + \epsilon c_{pg} uC\frac{\partial T}{\partial z} - \sum_i (-\Delta H_a)_i (1-\epsilon)\rho_p \frac{\partial \bar{q}_i}{\partial t} + \frac{2h_w}{R_i}(T - T_w) = 0 \quad (4)$$

Energy balance around the column wall is given by

$$c_{pw}\rho_w a_w \frac{\partial T_w}{\partial t} = 2\pi h_w R_i (T - T_w) - 2\pi U_w R_o (T_w - T_{amb}) \quad (5)$$

An accurate multicomponent adsorption equilibrium model is very crucial in modeling a multicomponent PSA separation. Many researchers have developed models to estimate multicomponent adsorption equilibrium. Simple models are obtained by extending the pure component isotherm equation to the multicomponent isotherm equation, which include the EL and LRC models. The models obtained from this approach have the main advantage of simplicity and are widely used for the design purposes (Cen and Yang, 1985; Yang and Doong, 1985). However, those models are thermodynamically inconsistent unless the monolayer saturation capacities of all components are equal.

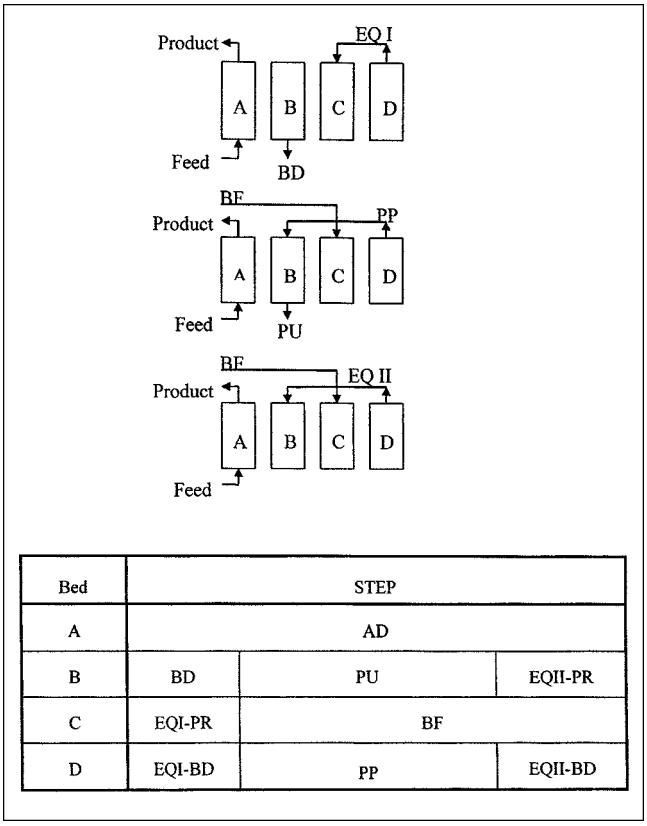

Bed	STEP		
A	AD		
B	BD	PU	EQII-PR
C	EQI-PR	BF	
D	EQI-BD	PP	EQII-BD

Figure 2. Flow direction and cycle sequences of H_2 PSA.

Another most successful model is derived from the thermodynamic solution theory. This model gave a good prediction for the variety of the multicomponent adsorption equilibrium. When the adsorbed phase is ideal, the theory is called as ideal adsorbed solution (IAS) theory, first proposed by Myers and Prausnitz (1965). The IAS theory defines the adsorption equilibrium between a gas mixture of N components and a specific adsorbent by a system of equations

$$Py_i = p_i^o(\Pi)\,x_i, \qquad i = 1, 2, \ldots, N \tag{6}$$

$$\Pi_1 = \Pi_2 = \ldots\ldots = \Pi_N \tag{7}$$

$$\Pi_i^* = \frac{\pi_i A}{RT} = \int_0^p \frac{q_i^*}{p}\,dp \tag{8}$$

$$\frac{1}{n_t} = \left[\sum_i \frac{x_i}{q_i^*(p_i^o)}\right] \tag{9}$$

$$n_i = n_t x_i \qquad i = 1, 2, \ldots, N \tag{10}$$

In this study, the Langmuir isotherm is applied as pure component adsorption equilibrium

$$q_i^* = \frac{q_{si} b_i p_i}{1 + b_i p_i} \tag{11}$$

Table 2. Operating Conditions of Experimental Runs

Run	P_H (atm)	P_L (atm)	ν_f* (cm/s)	ΔP** (atm)	t_{AD} (s)	Carbon/ Zeolite Ratio† (AC/ZE)
A	23.6	1.0	4	3	61	60/60
B	23.6	1.0	4	3	75	60/60
C	23.6	1.0	4	3	90	60/60
D	23.6	1.0	6	3	35	60/60
E	23.6	1.0	6	3	40	60/60
F	23.6	1.0	4	3	61	80/40
G	23.6	1.0	4	3	75	80/40
H	23.6	1.0	4	3	90	80/40
I	23.6	1.0	6	3	35	80/40
J	23.6	1.0	6	3	40	80/40
K	23.6	1.0	6	3	42	80/40
L	23.6	1.0	6	3	45	80/40
M	23.6	1.0	4	3	45	100/20
N	23.6	1.0	4	3	61	100/20
O	23.6	1.0	4	3	90	100/20
P	23.6	1.0	6	3	35	100/20
Q	23.6	1.0	6	3	50	100/20

*Superficial velocity.
**Pressure difference before and after provide purge step.
†Activated carbon layer height to zeolite 5A layer height (cm/cm).

where the parameters b_i and q_{si} depend on the temperature in the following way

$$b_i = b_{io}\exp(b_{i1}/T) \qquad q_{si} = a_{i,1} + a_{i,2}/T \tag{12}$$

The Langmuir isotherm parameters and the heat of adsorption are listed in Table 3. Applying the Langmuir isotherm, the spreading pressure of the component is given as

$$\Pi_i^* = q_{si}\ln(1 + b_i P) \tag{13}$$

The above system of algebraic equations is solved by the FastIAS scheme proposed by O'Brien and Myers (1988).

Figure 3 compares three adsorption equilibrium models, the extended Langmuir, LRC and the IAS theory with the experimental binary adsorption equilibrium of CH_4/CO, CO_2/CO, and CO_2/CH_4 on the activated carbon at 4,600 mm Hg, 298 K. As shown in Figure 3, the IAS theory gives most accurate predictions than the other models for the three binary systems. The prediction accuracy of the LRC model is not better than that of the EL model. The selectivity for the

Table 3. Langmuir Isotherm Parameters and Heat of Adsorption

		$a_{i,1}\times10^3$ (mol/g)	$a_{i,2}$ (K)	$b_{i,0}\times10^7$ (1/mm Hg)	$b_{i,1}$ (K)	$-\Delta H_a$ (cal/mol)
Activated Carbon	H_2	4.32	0.0	6.72	850.5	1,879
	CO	0.92	0.52	7.86	1,730.9	3,986
	CH_4	−1.78	1.98	26.60	1,446.7	4,482
	CO_2	−14.2	6.63	33.03	1,496.6	6,112
Zeolite	H_2	1.24	0.36	2.20	1,159.3	1,486
	CO	−0.58	0.83	2.53	2,616.3	6,954
	CH_4	−0.29	1.04	6.44	1,862.1	4,635
	CO_2	2.09	0.63	0.67	3,994.3	12,128

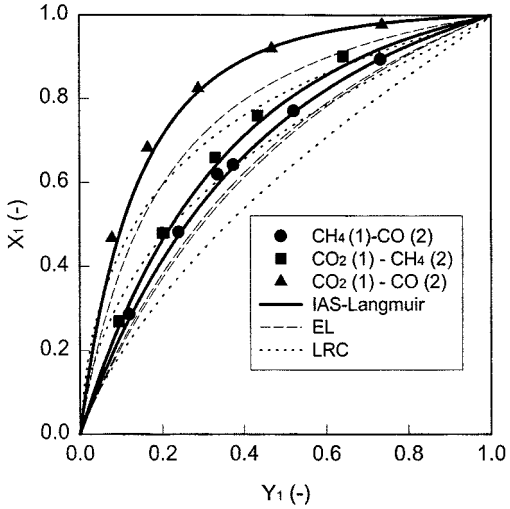

Figure 3. Experimental and model predictions for the binary adsorption equilibrium of CH_4/CO, CO_2/CH_4, and CO_2/CO on the activated carbon at 4,600 mm Hg, 298 K.

binary adsorption equilibrium predicted from the LRC model is given as follows

$$\frac{(1-y_1)^{1-n_2}}{y_1^{1-n_1}}\frac{q_{s1}b_1P^{n_1}}{q_{s2}b_2P^{n_2}} \tag{14}$$

The selectivity predicted from the LRC model varies from zero to infinity. That is, an azeotrope is predicted in the LRC model. It is not always true, especially in the present system.

The other multicomponent adsorption equilibrium of CO_2, CH_4, CO on Zeolite 5A were also well predicted with the IAS theory (Kim et al., 1998). Therefore, the IAS theory is used to represent the multicomponent adsorption equilibrium.

Mass-transfer coefficients of the impurities and hydrogen were determined from the breakthrough experiment (Park et al., 1998) and given in Table 1. Surface and Knudsen diffusion are dominant on activated carbon and surface diffusion is dominant on zeolite 5A (Doong and Yang, 1986, 1987). Therefore, the pressure dependence of the diffusivities can be neglected. Knudsen and surface diffusivities are dependent on the temperature. Temperature swing observed in the experiment was 40°C. Knudsen diffusivity is nearly constant over this temperature range. Surface diffusion is more strongly dependent on the temperature than Knudsen diffusion and also dependent on the surface coverage. However, here, the dependence of surface diffusivity on temperature and surface coverage was neglected for the first approximation and the mass-transfer coefficients of all components were set constant.

The heat-transfer rate between the wall and gas phase depends on the mass flux. Since the mass flux during a cycle is not constant, the heat-transfer rate is also not constant. Leva's correlation is inappropriate to estimate the heat-transfer coefficient, because it underestimates the heat-transfer coefficient at low mass flux. Thus, the correlation proposed by Yagi and Kunii (1960) was used to calculate the heat-transfer coefficient

$$Nu=\frac{h_w d_p}{k_g}=\frac{h_w^o d_p}{k_g}+\alpha_w PrRe_p,$$

$$Re_p=\frac{d_p u_f \rho_g}{\mu}<2{,}000 \tag{15}$$

$$h_w=h_w^o+\alpha_w\left(C_{pg}\rho_g u_f\right) \tag{16}$$

where h_w^o is the heat-transfer coefficient when the gas phase is stagnant and related to the thermal conductivity of the gas and solid phase. The second term of Eq. 15 represents the extra heat transfer caused by the gas flow. The exact value of α_w should be determined from the experiment, but, in this study, both the values of h_w^o, α_w were treated as fitting parameters. With the known values of the heat-transfer coefficients from the breakthrough experiment (Park et al., 1998), 3.3×10^{-3} and 1.8×10^{-3} cal/(cm^2·s·K) for the activated carbon and zeolite layer, respectively, the value of α_w was determined from Eq. 16 once the value of h_w^o was specified.

As shown in Figure 2, the effluent of the EQ I-BD, EQ II-BD, and PP steps are used as influent for the EQ I-PR, EQ II-PR, and purge steps. To track the transition behavior of all four beds requires a huge computational time. Therefore, we used only one bed to simulate this four-bed process. To describe bed connectivity, temporal effluent arrays (flow, composition, and temperature) from the process step are retained and later used when the bed is undergoing the appropriate process step. Temporal effluent arrays are stored at a predetermined time interval and quadratic interpolation is used when it becomes an input to a subsequent step. As mentioned in the experimental section, the products from each column enter the product storage vessel and then it is used as BF stream. Since the diameter of the pipe is small, it is assumed that the effluents of the adsorption, EQI-BD, PP, and EQII-BD steps are cooled to ambient temperature before they enter the other bed.

Boundary conditions for the ensuing cycles can be written as follows

BF step: $y_i(L,t)=\bar{y}_{i,p}, \quad T(L,t)=T_F$ (17)

AD step: $y_i(0,t)=y_{i,F}, \quad T(0,t)=T_F, \quad u(0,t)=u_H$ (18)

EQ I-BD, PP and EQ II-BD step: $u(0,t)=0$ (19)

BD step: $u(L,t)=0,$ (20)

Purge step: $y_i(L,t)=y_{i,PP}, \quad T(L,t)=T_F,$

$$u(L,t)=u_{PP}\frac{P_{PP}}{P_{PU}} \tag{21}$$

EQ II = PR step: $y_i(L,t)=y_{i,\mathrm{EQII\text{-}BD}}, \quad T(L,t)=T_F$ (22)

EQ I = PR step: $y_i(L,t)=y_{i,\mathrm{EQI\text{-}BD}}, \quad T(L,t)=T_F$ (23)

In addition to the above boundary conditions for the temperature and concentration, boundary conditions for the pressure or velocity during the pressure changing steps are

necessary to solve the system of the differential equations. Kumar et al. (1994) and Mahle et al. (1996) specified the velocity at the open end of the bed. The velocity at the open end is obtained from the valve equation, which relates the volumetric flow rate to the pressure decrease through the valve. This approach is realistic, but requires much longer computational time than specifying the pressure (Yang, 1987).

Rather than specifying the velocity, Yang and Doong (1985) and Cen and Yang (1985) expressed the pressure explicitly with time. Specifying the pressure history, one can reduce the calculation load (Yang, 1987). However, the moles flowing out from one bed may not be balanced to the moles flowing into the other bed at the pressure equalization steps. Thus, in this study, the pressure at the end of the pressure equalization steps were iterated until the moles transferred between the two beds balance each other under the assumption that the pressure changes linearly with time. That is, after one cycle calculation is completed, the pressures after the first and second pressure equalization steps are estimated from the following equations

$$N^k_{\text{EQI-BD}}\frac{P_{AD}-P^{k+1}_{\text{EQI}}}{P_{AD}-P^{k}_{\text{EQI}}}=N^k_{\text{EQI-PR}}\frac{P^{k+1}_{\text{EQI}}-P^{k+1}_{\text{EQII}}}{P^{k}_{\text{EQI}}-P^{k}_{\text{EQII}}} \quad (24)$$

$$N^k_{\text{EQII-BD}}\frac{P^{k+1}_{\text{EQI}}-\Delta P-P^{k+1}_{\text{EQII}}}{P^{k}_{\text{EQI}}-\Delta P-P^{k}_{\text{EQII}}}=N^k_{\text{EQII}-\text{PR}}\frac{P^{k+1}_{\text{EQII}}-P_L}{P^{k}_{\text{EQII}}-P_L} \quad (25)$$

where ΔP is the pressure difference before and after the provide-purge step. $N^k_{\text{EQI}-\text{BD}}$, $N^k_{\text{EQII}-\text{BD}}$, $N^K_{\text{EQI}-\text{PR}}$, $N^k_{\text{EQII}-\text{PR}}$ are the total moles leaving and entering the bed during the pressure equalization steps at the kth cycle calculation under the assumption that the pressure is the linear function of time. Using the above procedure, the complete pressure history is obtained without measuring it through the experiment for the different values of ΔP.

To solve the above system of partial differential equations, the spatial derivatives are divided using a backward difference scheme, and the resulting ordinary differential equations are solved with the GEAR method. We used the personal computer (PC, pentium 166 MHz) to solve the above differential equations. The CPU time for a cycle calculation, of which the cycle time was 4 min, was 72 s.

Results and Discussion

Experimental and simulation results from the run G

In this section, general characteristics of the process are investigated based on the experimental and simulation results for run G. At this run, the height of activated carbon layer was 80 cm, the adsorption step time was 75 s, the decrease of pressure during the PP step was 3 atm, and the superficial velocity of feed was 4 cm/s. Figure 4 shows the pressure history of the first column during one cycle for run G. As shown in Figure 4, the adsorption and purge pressures were 23.6 atm and 1 atm, respectively. The pressures after the first and second pressure equalization steps were about 13.7 atm and 5.9 atm, respectively. At all steps except the BF step, the pressure changes almost linearly. In this system, the combined thermal and concentration wave was observed (Park et al., 1998) so that the movement of the concentration

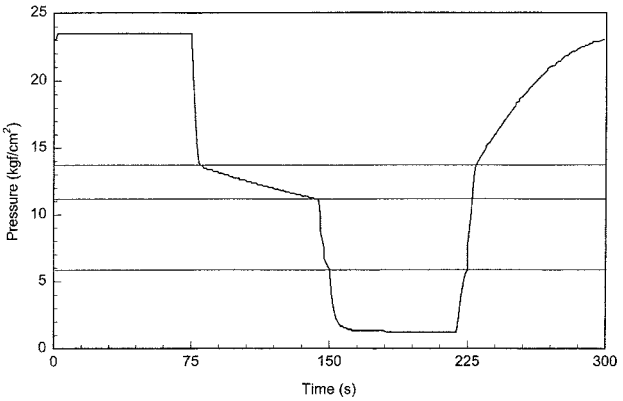

Figure 4. Pressure history during one cycle at run G.

Superficial velocity of feed: 4 cm/s, adsorption step time: 75 s; carbon-to-zeolite ratio: 2.

wave front can be inferred from the temperature profiles. Bed temperature profiles for run G at the end of the adsorption (AD), second pressure equalization (EQII-BD), purge (PU), and backfill (BF) steps in the cyclic steady state are given in Figure 5b. After the adsorption step, the temperature in the activated carbon layer rises up to 30°C because of the adsorption of carbon dioxide, methane, and carbon monoxide. A small temperature rise in the zeolite layer implies that some impurities are adsorbed there. After the second pressure equalization step, the temperature wave fronts of both layers shifted to the product end and the temperature at the feed end decreased. This is because the impurities at the feed end are desorbed and re-adsorbed at the product end. The bed

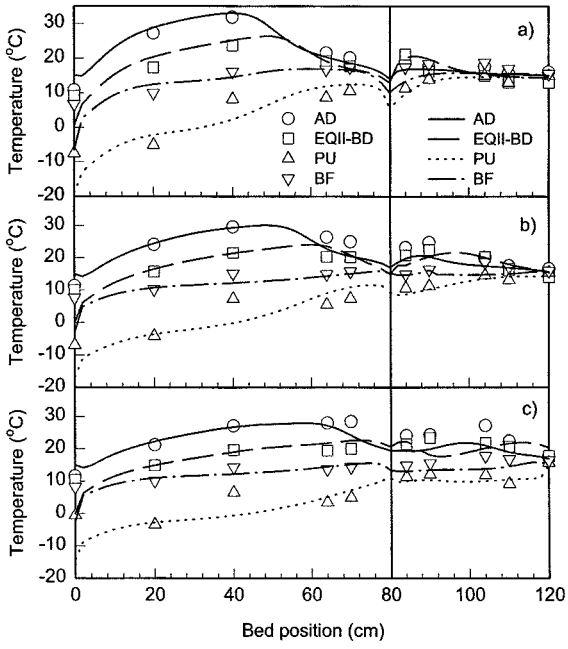

Figure 5. Bed temperature profiles in runs F, G, and H.

The adsorption step times of the runs are: (a) 60 s, (b) 75 s, (c) 90 s, superficial velocity and carbon-to-zeolite ratio are fixed at 4 cm/s, 2 respectively; symbol: experiment, line: simulated.

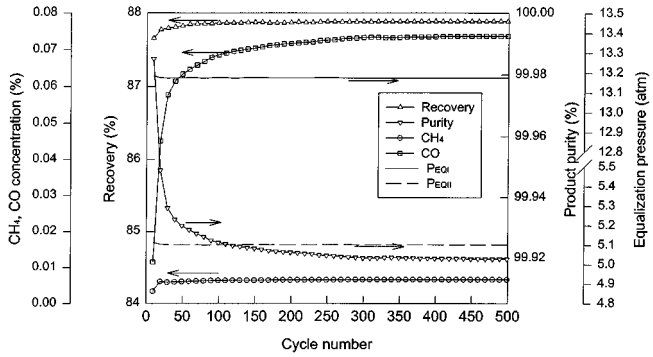

Figure 6. Changes in product purity, recovery, pressures after the first and second pressure equalization steps, and impurity concentration with the cycle number for run G.

Superficial velocity of feed: 4 cm/s; adsorption step time: 75 s; carbon-to-zeolite ratio: 2.

temperature further decreased during the purge step due to the desorption of impurities. The maximum temperature swing observed in this run was about 30°C at the carbon layer. It is seen that the prediction from the model quite well represents the experimentally observed results.

Figure 6 shows transient behaviors of the product purity, recovery, impurity concentration, and pressures at the end of the first and second pressure equalization steps, which was obtained from the simulation for run G. It is seen in Figure 6 that the pressures at the end of the pressure equalization steps converge to the steady-state values after ten cycles. The values of P_{EQI} and P_{EQII} were about 13.2 atm and 5.1 atm, respectively. Those values were close to the value observed in the experiment. These validate the iteration scheme proposed to calculate the pressures at the end of the pressure equalization steps.

While the P_{EQI} and P_{EQII} converge to the steady-state values after the 10th cycle, the product recovery converged to a steady-state value after the 50th cycle. The main impurity of the product was carbon monoxide. As the cycle number increases, the concentration of carbon monoxide increases, and, consequently, the product purity gradually decreases. The process reaches the cyclic steady state after the 500th cycle. It is impractical to check the product purity and recovery at every cycle in order to determine the cyclic steady state. Thus, in this study, it was assumed that the cyclic steady state has been attained if the changes of product purity and recovery were less than 5×10^{-5}% and 5×10^{-3}% between the subsequent two cycles, respectively. For this illustrative simulation run, the criterion was satisfied at the 161st cycle. The change of product purity during next 340 cycles was about 0.003%. That is, the real cyclic steady state was reasonably well predicted with the above criteria. In the experiment, the number of cycles required to reach the cyclic steady state was 37 cycles. The cyclic steady state was achieved much faster in the experiment. This is because the criteria for the cyclic steady state and the initial conditions of experiment and simulation were different. In the experiment, we assumed that the cyclic steady state was reached when the product purity changed no more than 50 ppm in the subsequent two cycles. However, in simulation, the criterion was 0.5 ppm. In addition to that, while the simulation started under the assumption that the bed was clean, the experiment was conducted without regeneration after every cycle run so that the initial bed was not clean. Therefore, the direct comparison between two cycle numbers is impossible. However, it is interesting that the purity predicted in the simulation changes no more than 50 ppm after 50 cycles.

Carbon dioxide has a highly favorable isotherm on the zeolite, so that it is not desorbed easily by decreasing the system pressure and it accumulates in the zeolite layer. Thus, it has been believed that carbon dioxide has to be removed in the activated carbon layer completely before it enters the zeolite layer (Chlendi and Tondeur, 1995). Figure 7 represents the gas and solid phase concentration profiles at the end of the EQII-BD step at the 161st, 300th, and 500th cycles. The EQII-BD step is the last cocurrent depressurization step, so that the bed is most contaminated after this step. Whether carbon dioxide is completely removed or not in the activated carbon layer is seen in Figure 7. Figure 7 shows that quite a large amount of carbon dioxide is adsorbed in the zeolite layer even though the gas-phase concentration of carbon dioxide is extremely low. When carbon dioxide enters the zeolite layer, it should be carefully investigated whether it breaks through the whole bed or not. According to Levan (1995), the more favorable the isotherm is, and the more cycles are required until the process reaches the cyclic steady state. Figure 6 confirmed that the real cyclic steady state has been attained at the 500th cycle for this simulation run G. Figure 7 shows that carbon dioxide does not break through the whole bed at the 500th cycle at cyclic steady state. While the solid-phase concentration profiles of carbon dioxide and carbon monoxide in the zeolite layer at the 161st and 500th cycle change a little,

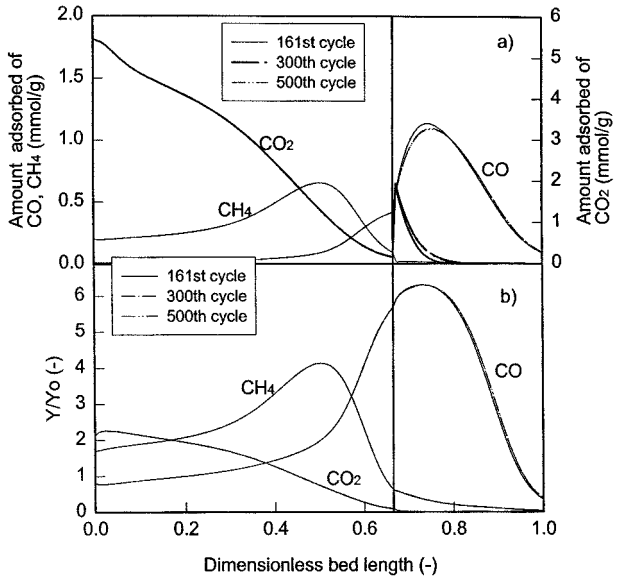

Figure 7. (a) Solid and (b) gas-phase concentration profiles at the end of the EQII-BD step for run G.

Superficial velocity of feed: 4 cm/s; adsorption step time: 75 s; carbon-to-zeolite ratio: 2; after the 161st cycle, the change of the recovery and purity between subsequent two cycles are no more than 0.005%, 0.5 ppm, respectively.

all the concentration profiles in the activated carbon layer at two cycles coincide with each other. Since no adsorption isotherms of the impurities on the activated carbon are so favorable as that of the carbon dioxide in the zeolite, the other components reach the cyclic steady state more quickly than carbon dioxide in the zeolite layer. It is also noted in Figure 7 that the amount adsorbed of carbon monoxide in the zeolite layer does not show the sharp decrease at the part contaminated with carbon dioxide. Since a small amount of carbon dioxide neither accumulates nor reduces the amount adsorbed of carbon monoxide, one should not need to completely remove it with activated carbon.

Performance curve

Three different quantities, that is, product purity, product recovery, and process productivity, define the performance of the PSA process. The above three quantities depend on the operating conditions of the PSA processes in a complicated manner. If the experimental conditions are chosen arbitrarily, then a direct comparison between different processes is difficult.

In any process, the productivity is given by the product of the recovery, purity, and the feed flow rate. Therefore, at a constant feed flow rate, the productivity is solely determined by the recovery and purity. This means that it can be determined which process is better by comparing the purity and recovery at the fixed feed flow rate. This makes the comparison between the process alternatives easy.

At a constant feed flow rate, while the bed utilization increases with the adsorption step time, the product purity decreases due to the breakthrough of the impurities. When the adsorption step time is extremely short, the breakthrough of the impurities does not take place at all. In this range of the adsorption step time, the small increase of the adsorption step time causes no decrease of the product purity. However, if the adsorption step time exceeds a threshold value, the increase of the adsorption step time always causes the decrease of the purity. Above this threshold value of the adsorption step time, the recovery and purity has a one to one relation except for some special processes (Kikkinides et al., 1995), where multiple cyclic steady state occur according to the operating conditions. That is, in the ordinary process, a specific purity always corresponds to a specific recovery. While performing the experiment with the adsorption step time at the given feed flow rate, a relation between the recovery and purity is obtained. The curves obtained in this way represent the process performance characteristics, so it could be called a performance curve.

The runs F, G, and H in Table 2 were the experiments which investigated the relation of purity and recovery when the height of the activated carbon layer was 80 cm and the superficial velocity was 4 cm/s. The adsorption step times for the runs F, G, and H are 61 s, 75 s and 90 s, respectively. Figure 5 shows the experimentally measured bed temperature profiles at the cyclic steady state and the predictions from the model. The general trends are kept in the three runs. It is seen that the temperature wave fronts shift to the column exit as the adsorption time increases. The agreement between the experiment and theoretical prediction is excellent. This validates the present model.

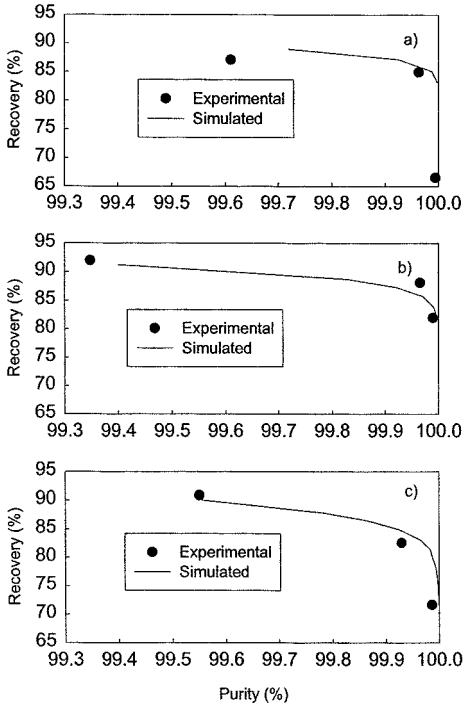

Figure 8. Performance with the carbon-to-zeolite ratio: (a) 1, (b) 2, (c) 5.

Superficial velocity of feed: 4 cm/s; cycle time varies; total bed height: 120 cm.

The relation between the purity and recovery obtained in the series of experimental runs F, G, and H is shown in Figure 8b. As expected, the recovery can be increased at the expense of the purity and the purity decreases rapidly above certain recovery. The agreement between the experiment and model prediction is good. It is noted from Figure 8b that about 84% of hydrogen can be recovered with 99.99% purity. As mentioned above, this curve is obtained at the superficial velocity of 4 cm/s. Therefore, the curve represents not only the purity-recovery relation, but also the purity-productivity. The productivity is obtained by multiplying the recovery, purity, and the feed flow rate.

Optimum carbon-to-zeolite ratio

To investigate the effect of the each layer's height on the process performance, performance curves at a different carbon-to-zeolite ratio were obtained. Figure 8 shows the performance curves when the carbon-to-zeolite ratio are 1, 2, and 5. The model quite accurately predicted the experimental data at all the carbon-to-zeolite ratios. Both the experimental data and model prediction revealed that height ratio of 5 gave a worst recovery at high purity. Figures 9 and 10 show the solid-phase loading and the gas-phase concentration profiles at the end of EQII-BD step with the activated carbon layer height, respectively. From Figure 9a, it is seen that a small amount of carbon dioxide penetrates into the zeolite layer even though the height of the activated carbon layer is 100 cm. As the height of the activated carbon layer decreases, the amount of carbon dioxide penetrating to the

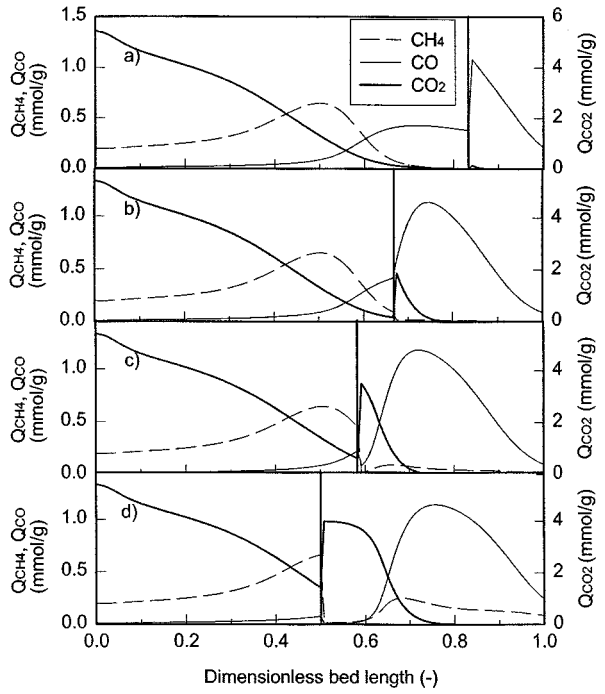

Figure 9. Simulated solid-phase concentration with the carbon-to-zeolite ratio at the end of the EQ II-BD step: (a) 5, (b) 2, (c) 1.4, (d) 1.

Superficial velocity of feed: 4 cm/s; adsorption step time: 75 s; total bed height: 120 cm.

zeolite layer increases. However, the decrease of amount adsorbed of carbon monoxide caused by competition with carbon dioxide is not too serious before a substantial amount of carbon dioxide penetrates into zeolite layer. Therefore, one should not need to remove carbon dioxide completely in the activated carbon layer, and to do so is a very difficult task, as shown in Figure 9a. However, if the activated carbon layer is too short, then a substantial amount of carbon dioxide enters the zeolite layer, which reduces the effectiveness of zeolite in removing carbon monoxide and methane as shown in Figure 9d. Figure 10 shows the gas-phase concentration profiles after the second pressure equalization step. It is seen in Figure 10 that while the concentration of carbon monoxide at the column exit shows a minimum, that of methane at the product end increases continuously with the decrease of the carbon-to-zeolite ratio. This means that the activated carbon is more efficient to remove methane than the zeolite. As for the carbon monoxide, the zeolite is more efficient so that the concentration of carbon monoxide first decreases with the decrease of the carbon-to-zeolite ratio and then increases because carbon dioxide contaminates the zeolite layer at the much lower carbon-to-zeolite ratio. It is seen in Figure 10 that 2 of the carbon-to-zeolite ratio gives a higher product purity. It is also noted that the concentration profiles of carbon dioxide and methane in the activated carbon layer were slightly affected by the adsorbents ratio, while the concentrations of methane and carbon monoxide in zeolite were greatly affected by the ratio of the adsorbents.

Even if the 2 of carbon-to-zeolite ratio gives the purest product, it does not mean that the process performance is highest at that carbon-to-zeolite ratio, because the recovery and productivity also should be taken into account. Those comparisons could be made easily with the performance curves. Figure 11 shows performance curves obtained from the simulation with the carbon layer heights. Since the superficial velocity was fixed at all simulations, the productivity of the process was proportional to the recovery at the given purity. The height of the carbon layer that gives the highest recovery at the given purity is optimal bed layering. As shown in Figure 11, when the extremely high purity of the product is desired, the carbon-to-zeolite ratio should be 1, because it gives the highest recovery. However, if 99.99% of hydrogen is desired, the carbon-to-zeolite ratio should be 1.4. This means that the optimum carbon-to-zeolite ratio changes with the product purity.

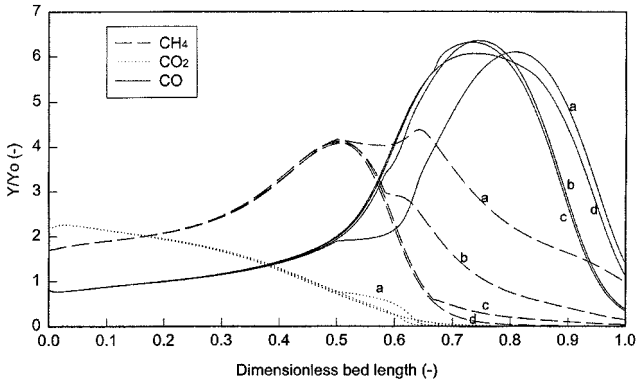

Figure 10. Simulated gas-phase concentration at the end of the EQII-BD step with the carbon-to-zeolite ratio: (a) 1, (b) 1.4, (c) 2, (d) 5.

Superficial velocity of feed: 4 cm/s; adsorption step time: 75 s; total bed height: 120 cm.

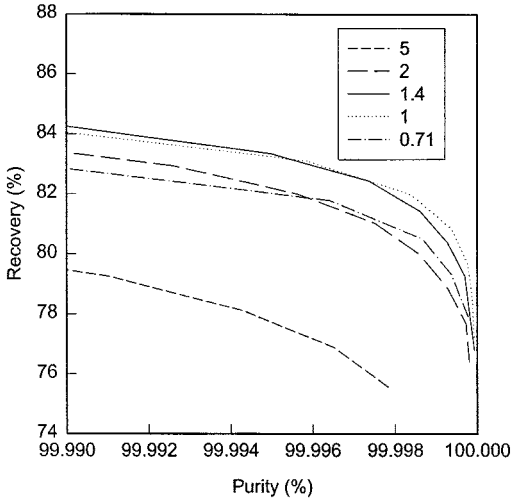

Figure 11. Simulated performance at different carbon-to-zeolite ratio.

The curves were generated by varying the cycle time at the constant superficial velocity of feed: 4 cm/s; total bed height: 120 cm.

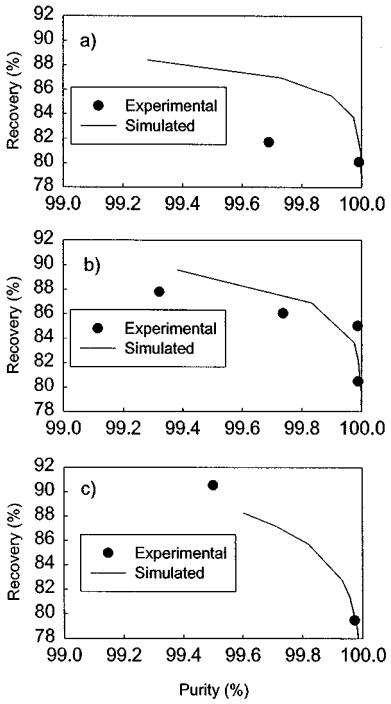

Figure 12. Performance at different carbon-to-zeolite ratio: (a) 1, (b) 2, (c) 5.

The curves were generated by varying the cycle time at the constant superficial velocity: 6 cm/s; total bed height: 120 cm.

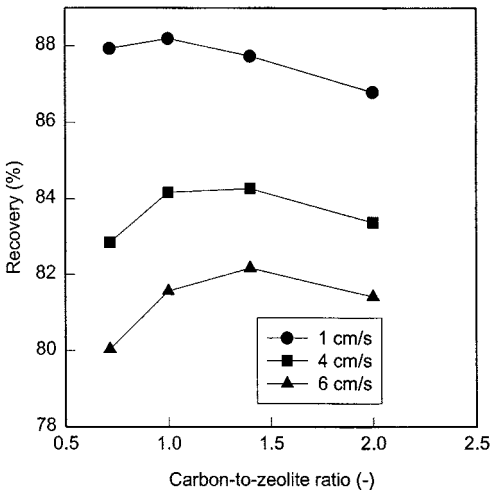

Figure 13. Effects of the superficial velocity on the process performance and optimum carbon-to-zeolite ratio.

Recovery when the product purity is 99.99%, interpolated from the simulated performance curves similar to Figure 11; total bed height: 120 cm.

Effects of superficial velocity on process performance and optimal bed layering

If higher productivity is desired at the same process, the superficial velocity has to be increased. However, as the superficial velocity increases, the mass-transfer zones of impurities are broadened so that the recovery decreases at the given purity. The productivity is important, because it is related to the capital cost of the process. On the other hand, the recovery is important, because it is related to the production cost. These two points have to be considered in designing the PSA process. The productivity and recovery are not improved simultaneously by only increasing the superficial velocity of the feed. To know the relation between the recovery and productivity is important to operate the process economically. For that purpose, experiments were made at the superficial velocity of 6 cm/s. The results are shown in Figure 12 with the theoretical prediction. The theoretical model reasonably predicted the experimental results. The recovery was the worst when the carbon-to-zeolite ratio was 5.

According to Park et al. (1998), the mass-transfer zone of carbon dioxide becomes much broader than those of methane and carbon monoxide with the increase of the superficial velocity of feed. That makes the optimum carbon-to-zeolite ratio increase with the superficial velocity. Figure 13 shows the process performance with the activated carbon layer height at three different superficial velocities of 1 cm/s, 4 cm/s, and 6 cm/s. The recovery in Figure 13 represents the recovery when the product purity is 99.99%, which was obtained by interpolating the simulation results. As shown in Figure 13, the process performance decreases with the increase of the superficial velocity at all the activated carbon layer heights. As the superficial velocity of feed increases from 1 cm/s to 4 cm/s, the optimum carbon-to-zeolite ratio increases from 1 to 1.4. However, the optimum activated to zeolite ratio at the superficial velocities of 4 cm/s and 6 cm/s are almost the same.

The productivity of the process is proportional to the superficial velocity of feed. It is seen in Figure 13 that the recovery decreases about 4% when the superficial velocity of feed increases from 1 cm/s to 4 cm/s. On the other hand, the recovery decreases about 2% when the superficial velocity increases from 4 cm/s to 6 cm/s. The decrease of the recovery caused by the increase of the superficial velocity is severe at the higher productivity. That is, if one wants to increase the productivity beyond a certain amount, then the recovery decreases drastically. In this case, the value of high productivity, low capital cost, is diminished by the high production cost. Contrary to that, though the productivity is decreased to improve the recovery, the recovery does not increase so much below certain productivity. So, there is an economical superficial velocity.

Effects of heat-transfer resistance

As the bed diameter increases, heat transfer to the environment becomes worse so that the process approaches an adiabatic process. If this happens, the adsorption takes place in the warmer bed and the regeneration takes place in the colder bed. This results in the decrease of the process performance and the shift in the optimum carbon-to-zeolite ratio. The poor heat dissipation associated with the increase of the bed diameter was simulated by decreasing the heat-transfer coefficient, while fixing the bed diameter because two extreme cases, isothermal and adiabatic conditions, can be easily represented by doing so. Two heat-transfer coefficients, h_w and U_w, define the heat-transfer characteristics of the sys-

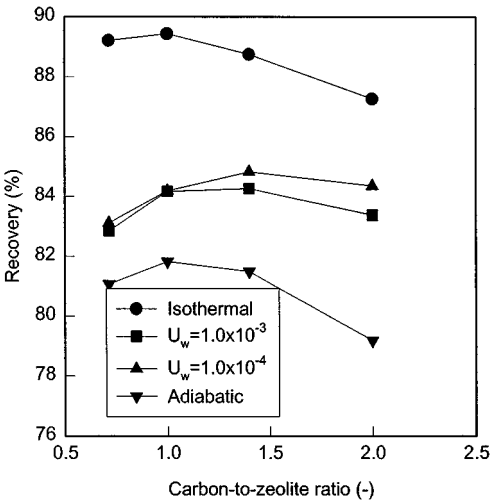

Figure 14. Effects of the heat-transfer resistance on the process performance and optimum carbon-to-zeolite ratio.

Recovery when the product purity is 99.99%, interpolated from the simulated performance curves similar to Figure 11; total bed height: 120 cm.

tem. While the inner wall heat-transfer coefficient h_w (cal/cm^2·s·K) changes according to Eq. 16, the outer wall heat-transfer coefficient *Uw* (cal/cm^2·s·K) is constant. Thus, it is more convenient to use U_w to represent the heat-transfer characteristics of the simulation run. Figure 14 shows the process performance with the height of the activated carbon layer with the heat-transfer coefficients at the outer wall surface (U_w). Four values of U_w were considered that cover from the isothermal to adiabatic conditions: infinity, 1.0×10^{-3}, 1.0×10^{-4}, 0.0 cal/(cm^2·s·K). The 1.0×10^{-3} cal/(cm^2·s·K) of U_w is the value obtained in our present experimental apparatus. The heat-transfer coefficient at the inner wall surface (h_w) is given by Eq. 16. The values of h_w^o and α_w were obtained by scaling the values obtained in the experimental apparatus by the factor $U_w/1.0\times10^{-3}$. That is, when the U_w is 1.0×10^{-3} cal/(cm^2·s·K), the factor $U_w/1.0\times10^{-3}$ is 1 so that h_w^o and α_w are the same as those in our experimental apparatus. If the U_w is 1.0×10^{-4} cal/(cm^2·s·K), the factor is 1/10 so that the h_w^o and α_w are also 1/10 of those values obtained in our experimental apparatus. Also, if U_w is infinity or 0, then h_w^o and α_w are infinity or 0, too. In these simulation studies, the superficial velocity of feed was 4 cm/s. The recovery shown in Figure 14 represents the recovery when the product purity is 99.99%. As shown in Figure 14, the poorer the heat transfer is, and the worse the process performance is, in general. However, the reverse is also observed, that is, the performance obtained at 1.0×10^{-3} cal/(cm^2·s·K) of U_w is worse than that obtained at U_w of 1.0×10^{-4} cal/(cm^2·s·K).

The optimum carbon-to-zeolite ratio increases from about 1 to 1.4 as the heat-transfer resistance increases from zero to a finite value. With the increase of the heat-transfer resistance, the activated carbon layer experiences a much more severe temperature swing during a cycle because more amounts of impurities are adsorbed and desorbed there than in the zeolite layer. Thus, the effectiveness of the activated carbon is more reduced than that of the zeolite so that more amounts of the activated carbon are required at higher heat-transfer resistance. However, this general behavior breaks in the adiabatic conditions. As shown in Figure 14, the optimum carbon-to-zeolite ratio decreases from 1.4 to 1 as the heat-transfer resistance increases from the finite value to infinity. This could be understood looking over the temperature profile developing in the bed with the heat-transfer resistance. Figure 15 shows the temperature and gas-phase concentrations profiles at the end of EQII-BD step with the heat-transfer resistance. The carbon-to-zeolite ratio was 1.4 and the adsorption step time was 40 s. When the heat-transfer resistance is finite, the temperature in the activated carbon layer increases a lot with the heat-transfer resistance, but that in the zeolite layer does not increase so much as in the activated carbon layer. That explains the increase of the optimum carbon-to-zeolite with the heat-transfer resistance when the heat-transfer resistance is finite. When the heat-transfer resistance is infinity, the temperature in the zeolite also increases a lot, so that much of the adsorption capacity of zeolite is lost at the adiabatic conditions. This results in the decrease of the optimum carbon-to-zeolite ratio at the adiabatic conditions.

The increase of the process performance with the decrease of heat transfer rate from 1.0×10^{-3} cal/(cm^2·s·K) to 1.0×10^{-4} cal/(cm^2·s·K), could be understood from Figure 15. Comparing the concentration profiles obtained at 1.0×10^{-3} cal/(cm^2·s·K) of U_w to that obtained at 1.0×10^{-4} cal/(cm^2·s·K) of U_w, more steep concentration profiles are observed at higher heat-transfer resistance. Since a smaller amount of hydrogen is released during the subsequent blowdown step if

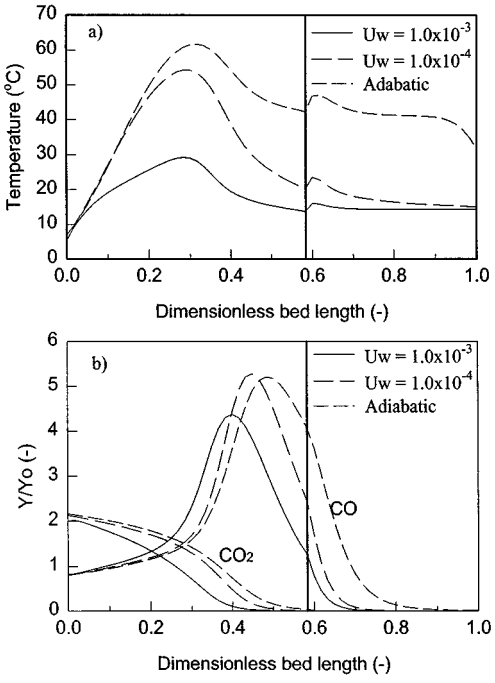

Figure 15. (a) Temperature and (b) gas-phase concentration at the end of EQII-BD with the heat-transfer resistance.

Superficial velocity: 4 cm/s; adsorption step time: 40 s.

the concentration profile is steep, higher recovery is obtained at higher heat-transfer resistance. In addition to this, since the wave fronts of carbon monoxide at two heat-transfer resistances are close to each other, the difference of purity between two could be small.

Conclusions

The process performances of the four-bed H_2 PSA process using layered beds were investigated experimentally and theoretically. The experimental conditions like feed composition and adsorption pressure resembled the reformer offstream's conditions. The roles of the height of the activated carbon layer, the superficial velocity of feed, and the heat-transfer resistance on the process performance were assessed. The nonisothermal, bulk separation PSA model adopted the linear driving force approximation for the particle uptake and the ideal adsorbed solution (IAS) model to represent multicomponent adsorption equilibrium. All the experimental results were well predicted by the theoretical model.

There was the optimum carbon-to-zeolite ratio, which maximize not only the recovery, but also the productivity at the given H_2 purity. According to the simulation studies, those values depend on the product purity, the superficial velocity of the feed, and the heat-transfer resistance. If purer product is desired, then the zeolite, the stronger adsorbent, has to be packed at a higher ratio.

The recovery at the given product purity decreased with the increase of the superficial velocity of feed, that is, with the increase of the productivity. The recovery sharply decreased above certain productivity. So, after carefully investigating the relation of the productivity and recovery, the superficial velocity of feed has to be chosen. The superficial velocity of feed also affected the optimum carbon-to-zeolite ratio. As the superficial velocity of feed increased, the optimum activated carbon layer height increased due to poor heat and mass transfers at a higher superficial velocity.

The heat-transfer resistance had bad influences on the process performance, in general. However, in some range of heat-transfer resistance, the phenomena that process performance increases with the increase of heat-transfer resistance were also observed. The effects of heat-transfer resistance on the optimum carbon-to-zeolite ratio were not simple. The optimum carbon-to-zeolite ratio increased with the increase of the heat-transfer resistance when the heat-transfer resistance is finite. However, at adiabatic conditions, the optimum carbon-to-zeolite ratio was lower than that at the nonisothermal conditions.

Notation

A = surface area of adsorbent, cm^2/g
a_w = cross-sectional area of column wall, cm^2
b_i = Langmuir isotherm parameter, L/mm HG
C = gas-phase concentration, mol/cm^3
c_{pg} = heat capacity of gas phase, cal/mol K
c_{ps} = heat capacity of particle, cal/g K
c_{pw} = heat capacity of column wall, cal/g K
d_p = diameter of particles, cm
$(-\Delta H_a)_i$ = heat of adsorption of ith component, cal/mol
k_g = thermal conductivity of gas, cal/cm·s·K
k_i = mass-transfer coefficient of ith component, L/s
n_t = total amount adsorbed of mixture, mol/g
p_i^o = pressure of the ith component that gives the same spreading pressure in the multicomponent equilibrium
P = pressure, mm Hg
P_{EQI}^k = pressure at the end of EQI-BD step at the kth cycle, mm Hg
P_{EQII}^k = pressure at the end of EQII-BD step at the kth cycle, mm Hg
P_{PP} = pressure of the effluent of the PP step, mm Hg
P_{PU} = purge step pressure, mm Hg
q_i^* = equilibrium amount adsorbed, mol/g
$\bar{q}_i$ = amount adsorbed of ith component, mol/g
q_{si} = saturation amount adsorbed of ith component, mol/g
R_i, R_o = inner and outer radius of column, cm
t = time, s
T = gas-phase temperature, K
T_{amb} = ambient temperature, K
T_F = temperature of feed, K
T_w = wall temperature, K
u = interstitial velocity, cm/s
u_f = superficial velocity, c/m
u_H = interstitial velocity of feed, cm/s
x = mol fraction of ith component in the adsorbed phase
y_i = mol fraction of ith component in the gas phase
$y_{i,\mathrm{EQI\text{-}BD}}$ = composition of ith component in the effluent of the EQI-BD step
$y_{i,\mathrm{EQII\text{-}BD}}$ = composition of ith component in the effluent of the EQII-BD step
$\bar{y}_{i,p}$ = average concentration of ith component in the product
$y_{i,PP}$ = composition of ith component in the PP effluent
z = distance along the length of the column, cm
ϵ = bed void fraction
Π_i = reduced spreading pressure defined in Eq. 8
ρ_g = gas density, g/cm^3
ρ_p = density of particles, g/cm^3
ρ_w = density of wall, g/cm^3

Literature Cited

Cen, P., and R. T. Yang, "Separation of a Five-Component Gas Mixture by Pressure Swing Adsorption," *Sep. Sci. Technol.*, **20**, 725 (1985).

Chlendi, M., and D. Tondeur, "Dynamic Behavior of Layered Columns in Pressure Swing Adsorption," *Gas. Sep. Purif.*, **9**, 231 (1995).

Chlendi, M., and D. Tondeur, "Dynamics of Two-Adsorbent Beds with Flow-Reversal for Gas Separation," *Fundamentals of Adsorption*, M. D. LeVan., ed., Kluwer Academic Publishers: Boston, p. 187 (1996).

Chlendi, M., D. Tondeur, and F. Rolland, "A Method to Obtain a Compact Representation of Process Performances from a Numerical Simulator: Example of Pressure Swing Adsorption for Hydrogen Production," *Gas Sep. Purif.*, **9**, 125 (1995).

Doong, S. J., and R. T. Yang, "Bulk Separation of Multicomponent Gas Mixture by Pressure Swing Adsorption: Pore/Surface Diffusion and Equilibrium Models," *AIChE J.*, **32**, 397 (1986).

Doong, S. J., and R. T. Yang, "Bidispersed Pore Diffusion Model for Zeolite Pressure Swing Adsorption," *AIChE J.*, **33**, 1045 (1987).

Feldbauer, G. F., "Depressurizing Technique for ΔP Adsorption Process," U.S. Patent No. 3,338,030 (1967).

Frey, D. D., "A Model of Adsorbent Behavior Applied to the Use of Layered Beds in Cycling Zone Adsorption," *Sep. Sci. Tech.*, **17**, 1485 (1983).

Kikkinides, E. S., V. I. Sikavitsas, and R. T. Yang, "Natural Gas Desulfurization by Adsorption: Feasibility and Multiplicity of Cyclic Steady State," *Ind. Eng. Chem. Res.*, **34**, 255 (1995).

Kim, J. N., and S. H. Cho, J. H. Park, J. D. Kim, and S. C. Ahn, "Multi-Component Adsorption Equilibrium of CO_2, CO, CH_4, H_2 Gases on Activated Carbon and Zeolite 5A," *Theory and Applications of Chem. Eng.*, **4**(2), 2493 (1998).

Klein, G., and T. Vermeulen, "Cyclic Performance of Layered Beds for Binary Ion Exchange," *AIChE Symp. Ser.*, **71**(152), 69 (1975).

Kumar, R., V. G. Fox, D. G. Hartzog, R. E. Larson, Y. C. Chen, P. A. Houghton, and T. Naheiri, "A Versatile Process Simulator for the Adsorptive Separations," *Chem. Eng. Sci.*, **49**, 3115 (1994).

Lee, C.-H., J. Yang, and H. Ahn, ''Effects of Carbon-to-Zeolite Ratio on Layered Bed H_2 PSA for Coke Oven Gas,'' *AIChE J*., **45**, 535 (1999).
Levan, M. D., ''Pressure Swing Adsorption: Equilibrium Theory for Purification and Enrichment,'' *Ind. Eng. Chem. Res.*, **34**, 2655 (1995).
Mahle, J. J., D. K. Friday, and M. D. Levan, ''Pressure Swing Adsorption for Air Purification. 1. Temperature Cycling and Role of Weakly Adsorbed Carrier Gas,'' *Ind. Eng. Chem. Res*., **35**, 2342 (1996).
Malek, A., and S. Farooq, ''Hydrogen Purification from Refinery Fuel Gas by Pressure Swing Adsorption,'' *AIChE J*., **44**, 1985 (1998).
Myers, A. L., and J. M. Prausnitz, ''Thermodynamics of Mixed Gas Adsorption,'' *AIChE J*., **11**, 121 (1965).
O'Brien, J. A., and A. L. Myers, ''A Comprehensive Technique for Equilibrium Calculations in Adsorbed Mixtures: The Generalized FastIAS Method,'' *Ind. Eng. Chem. Res*., **27**, 2085 (1988).
Park, J. H., J. N. Kim, S. H. Cho, J. D. Kim, and R. T. Yang, ''Adsorber Dynamics and Optimal Design of Layered Beds for Multicomponent Gas Adsorption,'' *Chem. Eng. Sci*., **53**(23), 3951 (1998).
Pigorini, G., and M. D. LeVan, ''Equilibrium Theory for Pressure Swing Adsorption: 2. Purification and Enrichment in Layered Beds,'' *Ind. Eng. Chem. Res*., **36**, 2296 (1997).
Ruthven, D. M., S. Farooq, and K. S. Knaebel, *Pressure Swing Adsorption*, VCH Publishers, New York (1994).
Tanczyk, M., and K. Warmuzinski, ''Multicomponent Pressure Swing Adsorption: I. Modelling of Large-Scale PSA Installations,'' *Chem. Eng. Proc*., **37**, 89 (1997).
Tanczyk, M., and K. Warmuzinski, ''Multicomponent Pressure Swing Adsorption: II. Experimental Verification of the Model,'' *Chem. Eng. Proc*., **37**, 301 (1998).
Wagner, J. H., ''Selective Adsorption Process,'' U.S. Patent No. 3,430,418 (1969).
Wankat, P. C., and D. Tondeur, ''Use of Multiple Sorbents in Pressure Swing Adsorption, Parametric Pumping and Cycling Zone Adsorption,'' *AIChE Symp. Ser*., **81**, 74 (1985).
Watson, C. F., R. D. Whitley, and M. I. Meyer, ''Multiple Zeolite Adsorbent Layers in Oxygen Separation,'' U.S. Patent No. 5,529,610 (1996).
Yagi, S., and D. Kunii, ''Studies on Heat Transfer Near Wall Surface in Packed Beds,'' *AIChE J*., **6**, 97 (1960).
Yang,. R. T., *Gas Separation by Adsorption Processes*, Butterworth, Boston (1987).
Yang, R. T., and S. J. Doong, ''Gas Separation by Pressure Swing Adsorption: A Pore Diffusion Model for Bulk Separation,'' *AIChE J*., **31**, 1829 (1985).

Manuscript received July 1, 1999, and revision received Nov. 24, 1999.